ISSN: 2281-1346

UNIVERSITÀ DI PAVIA
Department of Economics and Management

DEM Working Paper Series

NetVIX - A Network Volatility Index of Financial Markets

Daniel Felix Ahelegbey
(Università di Pavia)

Paolo Giudici
(Università di Pavia)

 # 192 (09-20)

Via San Felice, 5
I-27100 Pavia

economiaweb.unipv.it

NetVIX - A Network Volatility Index of Financial Markets

Daniel Felix Ahelegbey*, Paolo Giudici

Department of Economics and Management, University of Pavia, Italy

Abstract

We construct a network volatility index (NetVIX) via market interconnectedness and volatilities to measure global market turbulence. The NetVIX multiplicatively decomposes into an average volatility and a network amplifier index. It also additively decomposes into marginal volatility indices for measuring individual contribution to global turmoil. We apply our measure to study the relationship between the interconnectedness among 20 major stock markets and global market risks over the last two decades. The NetVIX is shown to be a novel approach to measuring global market risk, and an alternative to the VIX. The result shows that during crisis periods, particularly the tech-bubble, sub-prime, and COVID-19 pandemic, the interconnectedness of the markets amplifies average market risk more than 700 percent to cause a global meltdown. We find evidence that the highest risk-contributing markets to global meltdown are the US, Brazil, Hong Kong, France, and Germany.

Keywords: Centrality, COVID-19, Financial Crises, NetVIX, Turbulence, VAR, VIX

JEL: C11, C15, C51, C52, C55, C58, G01, G12

1. Introduction

The reaction of world economies to the global pandemic, caused by the widespread of the novel coronavirus (COVID-19), has reignited discussions on the fragility/resilience of the financial system to turbulent events of such magnitude. The debate has centered on whether a financial system with dense market interconnections is more vulnerable/resilient to shocks. On one hand, a considerable number of studies, beginning with Allen and Gale (2000) and Freixas et al. (2000), support the conclusion that densely connected markets increase resilience to financial turmoil. Their argument is based on the premise that higher connectedness provides an avenue for risk-sharing and diversification, thereby improving financial stability. In contrast, the works by Billio et al. (2012) and Blume et al. (2013) among others, show that dense financial interconnectedness increases market vulnerability for a systemic meltdown. While these two streams of literature provide an opposing conclusion on dense financial networks, recent studies by Haldane (2013) and Acemoglu et al. (2015) show that dense market connections may be viewed as a "robust-yet-fragile" system, in the sense that when the magnitude of shocks is within a certain range, the connections serve as shock-absorbers. Beyond a tipping point, these links act as shock-amplifying channels for a systemic meltdown.

*Corresponding author

Email addresses: danielfelix.ahelegbey@unipv.it (Daniel Felix Ahelegbey), paolo.giudici@unipv.it (Paolo Giudici)

The above debate inspires the first two research questions (RQ) of our current work: (RQ-1) does a densely interconnected market reduce or amplify financial risks?; and (RQ-2) Is there a threshold of market risk beyond which financial connections serves as shock-amplifiers?

Another topical issue in financial contagion studies is the identification of "systemically important" financial entities. These are countries, markets, or institutions whose failure affects the entire financial system. Identifying such entities is of great importance to regulators, policymakers, and researchers for the formulation of regulations. Various definitions of systemic importance have been put forth in the literature on network centrality measures (Bonacich, 1972; Faust, 1997; Freeman, 1978; Newman, 2010) and systemic risk (Avdjiev et al., 2019; Billio et al., 2012; Borgatti and Everett, 2006; Diebold and Yilmaz, 2014). To some, centrality is measured by the number of connected counterparties (degree). For others, the importance is portrayed by the location of an entity in the network (betweenness or closeness), and to some, centrality depends on the importance of an entity's counterparties (eigenvector). While these centrality measures have proved helpful, they only focus on the network properties without the relevance of an entity's risk, except Härdle et al. (2016).

The above open issue motivates our third research question: (RQ-3) which major market is central to the creation of global financial market risk?

We address the research questions by proposing a network volatility index (NetVIX) for measuring the level of turmoil/fears in financial markets. Our index is constructed by incorporating interconnectedness among markets, along with their volatilities. The latter is considered a measure of market uncertainty or fear, which can be proxied via standard deviation of returns. The interconnectedness among markets provide the channels for spillover propagation. Our approach to the construction of the NetVIX follows the Mahalanobis turbulence measure of Kritzman and Li (2010), and it is distinct from the systemic risk measures in (Adrian and Brunnermeier, 2016; Banulescu and Dumitrescu, 2015; Billio et al., 2012; Brownlees and Engle, 2017; Diebold and Yilmaz, 2014; Huang et al., 2012; Kritzman et al., 2011). The closest benchmark to our measure is the VIX, commonly referred to as the Chicago Board of Exchange volatility index, generally used for measuring the level of global market risk.

Our NetVIX has two important features. First, it multiplicatively decomposes into an average volatility index (AVX) and a network amplifier index (NetX). The latter measures the degree to which interconnectedness magnifies the average market risk to cause global turbulence. Secondly, it additively decomposes into marginal volatility indices (MVX) - for measuring individual contribution to global market turmoil. The MVX is shown to be helpful for policy decisions in terms of identifying markets with the highest contribution to global market turbulence and advancing interventions with the goal of ensuring financial stability.

The construction of the NetVIX and its features highlights our main contribution. We study the relationship between network density, the NetVIX, and the VIX to answer (RQ-1). We monitor the AVX and NetX to identify the threshold of market risks beyond which dense connections serve as shock-amplifiers, thus, answering (RQ-2). Finally, we study the MVX to identify the highest risk-contributing markets to global market risk, answering (RQ-3).

We formalize the derivation of the interconnectedness among stock market returns from a vector autoregressive with residual structural equations model (VAR-RSEM). That is, we model the dynamics of the returns by a reduced-form VAR with the residuals as a system of structural equations. Financial time series data usually exhibit contemporaneous dependencies as well as temporal lag relationships over time. The VAR-RSEM specification is designed to account for the contemporaneous, serial, and cross-lagged dependencies beyond what simple stylized fact from historical data can provide. Closely related models have in recent times been applied to infer financial contagion networks (see Ahelegbey et al., 2016a,b; Barigozzi and Brownlees, 2019; Basu and Michailidis, 2015; Bianchi et al., 2019; Billio et al., 2019, 2012; Diebold and Yilmaz, 2014). In a typical moderate to large VAR model, there are often too many parameters to estimate, compared to the available observations. A natural approach to overcome over-parametrization is via variable selection to produce parsimonious and sparse VAR models. The introduction of networks operationalized as graphical VAR models presents a convenient framework to achieve parsimony while providing explainable interactions in multivariate time series (Ahelegbey et al., 2016a).

In modeling financial contagion via networks, the underlying structure of interactions is often unknown and must be estimated from observed data. This is related to (graph) structural learning problem. To infer networks from multivariate financial time series, the widely applied competing methods include: Granger-causality (Billio et al., 2012); Lasso regularization methods (Basu and Michailidis, 2015; Kock and Callot, 2015); forecast error variance decomposition (Diebold and Yilmaz, 2014); and Bayesian graph structural learning methods (Ahelegbey et al., 2016a,b; Carvalho and West, 2007).

For structural learning, there is an inherent problem of uncertainty in the determination of the links between nodes. It is well known that the number of possible networks increases super-exponentially with the nodes, and there is usually a large number of valid networks that could explain the data approximately/equally well. Therefore, finding one single best network is a challenging model determination problem. Despite the wide application of the Granger-causality and Lasso regularization methods, there is a downside to their use for link identification due to their inability to quantify the uncertainty associated with the links in the network. The Bayesian graph structural learning, on the other hand, accounts for the uncertainty problem by incorporating relevant prior information where necessary. It also involves a search-and-score sampling scheme that aims at learning only those interactions that have a high marginal posterior probability. Sampling and averaging over high-scoring networks help to address the link uncertainty problem. In the current work, we build on the collapsed Gibbs algorithm in Ahelegbey et al. (2016a) by sampling the temporal dependence from its marginal distribution and the contemporaneous network from it's conditional distribution.

We apply our measure to study the dynamic interconnectedness among 20 major stock market indices, using daily prices from Bloomberg, covering January 2000 to June 2020. The result shows that dense interconnectedness increases market vulnerability. We document evidence of a significant relationship between the NetVIX and the VIX, with both indices providing similar signals about the direction of global market risk. We discover that during crisis periods (when average market volatility is usually higher than the 75th percentile), the network of stock market interconnectedness amplifies average market risk more than 700 percent to create a global meltdown. The result reveals that the highest risk-contributing markets to global turbulence are the US, Brazil, Hong Kong, France, and Germany.

The organization of the paper is as follows. In Section 2, we introduce our proposed network volatility index. We discuss VAR-RSEM model estimation and network selection in 3. We present a description of the data in Section 4 and report the results in Section 5. Section 6 concludes the paper with a final discussion.

2. Network Models and Network Volatility Index

Before presenting our network volatility index, we briefly introduce the general concept of network models and centrality measures.

2.1. Network Models and Centrality Measures

A network model is a convenient representation of statistical relationships among variables. It is defined by a set of nodes/variables joined by a set of links, describing the statistical relationships between pairs of variables. In many network models, the links are directed, representing statistical dependencies. In such representation, the relationships between variables can be summarized by a binary adjacency matrix $A \in \{0,1\}^{n\times n}$ or a weighted adjacency matrix $A^w \in \mathbb{R}^{n\times n}$, whose ij-th element is given by

$$A_{ij} = \begin{cases} 0, & \text{if} \quad Y_j \nrightarrow Y_i \\ 1, & \text{if} \quad Y_j \rightarrow Y_i \end{cases}, \qquad A^w_{ij} = \begin{cases} 0, & \text{if} \quad Y_j \nrightarrow Y_i \\ \alpha_{ij} \in \mathbb{R}, & \text{if} \quad Y_j \rightarrow Y_i \end{cases} \tag{1}$$

where $Y_j \nrightarrow Y_i$ means that Y_j does not influence Y_i, and $Y_j \rightarrow Y_i$ means Y_j influence Y_i.

A key feature of network models in financial contagion analysis is their usefulness in summarizing how densely connected are the institutions, and to identify which of them are critical (or central) to the robustness/fragility of the system. The density of a network is the number of links in the estimated network divided by the total number of possible links.

Node centrality addresses the question of how important a node/variable is in the network. Commonly discussed centrality measures include in-degree (number of in-bounds links), out-degree (number of out-bound links), authority, and hub scores. The authority score of node-i is a weighted sum of the power/hub score of the vertices with directed links towards node-i. The hub score of node-j is the weighted sum of the power/authority score of vertices with a directed link from node-j. The authority and hub scores can be obtained via eigendecomposition of (AA') and $(A'A)$. The absolute value of the eigenvectors associated with the largest eigenvalue of (AA') and $(A'A)$ is usually used as the authority and hub centrality score. A hub node usually has a large out-degree and an authority node has a large in-degree.

From a financial contagion viewpoint, nodes with high authority scores are mainly spillover "receivers", while high hub score nodes are spillover "transmitters". The above measures only focus on the inbound/outbound properties of the network without considering the relevance of institutional risks. Thus, they tend to overestimate/underestimate the importance of institutions in financial contagion analysis. In this paper, we construct an index for measuring the risk contribution of entities to the creation of global market risk via an econometric model.

2.2. Mahalanobis Distance Turbulence Index

We begin by presenting the Mahalanobis turbulence index of Kritzman and Li (2010), a statistical measure of financial turbulence which has been shown to provide a good representation of financial risks during periods of market turmoil. The index is given by

$$MTI_t = (Y_t - \mu)'\Sigma_Y^{-1}(Y_t - \mu) = \mathrm{tr}(\Sigma_Y^{-1} S_t) \tag{2}$$

where MTI_t is the Mahalanobis turbulence index at time t, Y_t is an $n \times 1$ vector of returns of n assets at time t, μ is an $n \times 1$ mean returns vector, Σ_Y is an $n \times n$ covariance matrix, tr() is the trace operator (the sum of the diagonal elements) and $S_t = (Y_t - \mu)(Y_t - \mu)'$ is the $n \times n$ inner product matrix. Equation (2) consists of two main components: the return partial correlations (captured by Σ_Y^{-1}) and the return standard deviations (captured by S_t). Note that, in the definition, the partial correlation matrix Σ_Y^{-1} does not have constraints on its elements. From a network perspective, this corresponds to a full weighted adjacency matrix.

2.3. Network Volatility Index (NetVIX)

From the Mahalanobis turbulence index in (2), we propose to replace the full weighted adjacency matrix used in the construction of Σ_Y^{-1} with a sparse weighted adjacency matrix. Thus, we extend the Mahalanobis turbulence measure, with the following proposition.

Proposition 1. *Let $Y = (Y_1, \ldots, Y_n)$ be return series of n-assets with risks $\sigma_Y = (\sigma_1, \ldots, \sigma_n)$ and let A^w be a weighted adjacency matrix . Assume $S_\sigma = \sigma_Y \sigma_Y'$ is the inner-product of risks, and $\Omega = (I + A^w)'(I + A^w)$ is their constrained precision matrix. We construct a network volatility index (NetVIX) by replacing in (2) Σ_Y^{-1} with Ω and S_t with S_σ:*

$$NetVIX \;=\; \frac{1}{n} tr(\Omega S_\sigma) \tag{3}$$

We illustrate the $NetVIX$ computation by considering $n = 3$ assets with return series $Y = (Y_i, Y_j, Y_k)$ and risks $\sigma_Y = (\sigma_i, \sigma_j, \sigma_k)$. Suppose A^w is a full weighted adjacency matrix:

$$I + A^w \;=\; \begin{pmatrix} 1 & a_{ij} & a_{ik} \\ a_{ji} & 1 & a_{jk} \\ a_{ki} & a_{kj} & 1 \end{pmatrix}, \qquad S_\sigma = \sigma_Y \sigma_Y' = \begin{pmatrix} \sigma_i^2 & \sigma_i\sigma_j & \sigma_i\sigma_k \\ \sigma_j\sigma_i & \sigma_j^2 & \sigma_j\sigma_k \\ \sigma_k\sigma_i & \sigma_k\sigma_j & \sigma_k^2 \end{pmatrix}$$

$$\Omega = \begin{pmatrix} 1 + a_{ji}^2 + a_{ki}^2 & a_{ij} + a_{ji} + a_{ki}a_{kj} & a_{ik} + a_{ji}a_{jk} + a_{ki} \\ a_{ij} + a_{ji} + a_{kj}a_{ki} & a_{ij}^2 + 1 + a_{kj}^2 & a_{ij}a_{ik} + a_{jk} + a_{kj} \\ a_{ik} + a_{jk}a_{ji} + a_{ki} & a_{ik}a_{ij} + a_{jk} + a_{kj} & a_{ik}^2 + a_{jk}^2 + 1 \end{pmatrix}$$

where $\Omega_{ij} = (a_{ij} + a_{ji} + a_{ki}a_{kj})$ is the weight of the relationship between Y_i and Y_j. Note that $\Omega_{ij} = 0$ if and only if Y_i and Y_j are not directly related (i.e., $a_{ij} = a_{ji} = 0$) and both variables are not related through Y_k (i.e., $a_{ki} = 0$ or $a_{kj} = 0$). In network terminology, $a_{ki} \neq 0$ means $Y_i \to Y_k$, thus, Y_k is a child of Y_i. Thus, if Y_k is a child of both Y_i and Y_j (i.e., $a_{ki}a_{kj} \neq 0$), then Y_i and Y_j must be parents of Y_k. So even though Y_i and Y_j may not be directly related, they are conditionally related through Y_k (i.e., $a_{ki}a_{kj} \neq 0 \implies a_{ki} \neq 0, a_{kj} \neq 0$).

By definition, Ω is a symmetric metric, i.e., $\Omega_{ij} = \Omega_{ji}$. Then, $NetVIX$ is computed as

$$\begin{aligned} NetVIX \;&=\; \frac{1}{n}\mathrm{tr}\,(\Omega S_\sigma) \;=\; \frac{1}{n}\mathrm{tr}\left[\begin{pmatrix} \Omega_{ii} & \Omega_{ij} & \Omega_{ik} \\ \Omega_{ji} & \Omega_{jj} & \Omega_{jk} \\ \Omega_{ki} & \Omega_{kj} & \Omega_{kk} \end{pmatrix}\begin{pmatrix} \sigma_i^2 & \sigma_i\sigma_j & \sigma_i\sigma_k \\ \sigma_j\sigma_i & \sigma_j^2 & \sigma_j\sigma_k \\ \sigma_k\sigma_i & \sigma_k\sigma_j & \sigma_k^2 \end{pmatrix}\right] \\ &=\; \frac{1}{n}\Big[\Omega_{ii}\sigma_i^2 + \Omega_{jj}\sigma_j^2 + \Omega_{kk}\sigma_k^2 + 2\Omega_{ij}\sigma_i\sigma_j + 2\Omega_{ik}\sigma_i\sigma_k + 2\Omega_{jk}\sigma_j\sigma_k\Big] \end{aligned} \tag{4}$$

By applying the above measure to a portfolio consisting of the world's major stock market indices, the $NetVIX$ produces a global index of financial market volatility taking into account the interconnectedness and risks of stock markets. It is therefore comparable to the volatility index by the Chicago Board Options Exchange (VIX) and can be used for measuring financial market risk. In this application, we study the relationship between network density, the $NetVIX$, and the VIX to answer (RQ-1).

An important property of our turbulence index is that it decomposes into the product two global indices: the volatility effect (Proposition 2) and the network effect (Proposition 3).

Proposition 2. *Let $\Sigma_A = \Omega^{-1}$ and $D_\Sigma = diag(\Sigma_A)$. From (3), we construct an average volatility index (AVX) by excluding the interactions among the different market assets in*

A^w. *This entails replacing in* (3) Ω *with* D_Σ^{-1}*:*

$$AVX \;=\; \frac{1}{n} tr\left(D_\Sigma^{-1} S_\sigma\right) \tag{5}$$

Note that $AVX = NetVIX$ when all off-diagonal elements in A^w are zeros. We remark that the AVX measure is similar to the magnitude surprise of Kinlaw and Turkington (2013).

Proposition 3. *From* (3)*, we can construct a network index ($NetX$) by excluding the average volatility index (AVX) from the $NetVIX$. This entails computing the following:*

$$NetX \;=\; \frac{NetVIX}{AVX} \;=\; \frac{tr\,(\Omega S_\sigma)}{tr\left(D_\Sigma^{-1} S_\sigma\right)}. \tag{6}$$

Note that $NetX$ measures the degree to which interconnectedness intensifies ($NetX > 1$) or weakens ($NetX < 1$) risks. The network effect can be likened to the correlation surprise in Kinlaw and Turkington (2013). It isolates the effect of interconnectedness in $NetVIX$.

Corollary 1. *From Proposition 3, the network volatility index is given by:*

$$NetVIX = NetX \cdot AVX \tag{7}$$

Thus, $NetVIX$ multiplicatively decomposes into an average volatility index (AVX) amplified by a network index ($NetX$) to produce a global level turmoil.

In this study, we monitor AVX and $NetX$ to identify the threshold of market risks beyond which dense connections serve as shock-amplifiers, and thus, answering (RQ-2).

Another important property of the $NetVIX$ is that it additively decomposes into local measures of marginal volatility indices obtained by computing the degree of responsiveness of $NetVIX$ to small changes in individual market risks as in the following:.

Proposition 4. *From* (3)*, we construct a marginal NetVIX index for security-i (MVX_i) as the partial derivative of $NetVIX$ with respect to asset-i's standard deviation:*

$$MVX_i = \frac{\partial(NetVIX)}{\partial \sigma_i} = \frac{2}{n}\Omega_{[i,:]}\sigma_Y \tag{8}$$

Proof. Recall from (4) that

$$\begin{aligned} NetVIX \;&=\; \frac{1}{n}\left[\Omega_{ii}\sigma_i^2 + \Omega_{jj}\sigma_j^2 + \Omega_{kk}\sigma_k^2 + 2\Omega_{ij}\sigma_i\sigma_j + 2\Omega_{ik}\sigma_i\sigma_k + 2\Omega_{jk}\sigma_j\sigma_k\right] \\ \frac{\partial(NetVIX)}{\partial\sigma_i} \;&=\; \frac{1}{n}\left[2\Omega_{ii}\sigma_i + 2\Omega_{ij}\sigma_j + 2\Omega_{ik}\sigma_k\right] \;=\; \frac{2}{n}\Omega_{[i,:]}\sigma_Y \end{aligned} \tag{9}$$

where $\Omega_{[i,:]}$ the i-th row of Ω. □

Corollary 2. *From Propositions 1 and 4, we have the following*

$$NetVIX = \frac{1}{2}\sum_i MVX_i\ \sigma_i \tag{10}$$

Thus, the $NetVIX$ can be seen as the sum of market risks weighted by their respective marginal volatility indices. Monitoring the MVX_i enables us to identify the highest contributing markets to global market meltdown, and answering (RQ-3).

3. Bayesian Graphical Model and Estimation

3.1. A VAR-RSEM Model

Let $Y_t = (Y_{1,t}, \ldots, Y_{n,t})$ be an n-variable vector of observed market returns at time t, where $Y_{i,t}$ is the time series of variable-i at time t. We model the dynamics of Y_t as a vector autoregression residual structural equations model (VAR-RSEM) given by

$$Y_t = \sum_{k=1}^{p} B_k \, Y_{t-k} + U_t \tag{11}$$

$$U_t = B_0 \, U_t + \varepsilon_t \tag{12}$$

where p is the lag order, B_k is a coefficients matrix such that $B_{i,j|k}$ capture the effect of Y_j on Y_i with a lag of k, U_t is a vector of residuals independent and identically normal with covariance matrix Σ_u, B_0 is also a coefficients matrix such that $B_{i,j|0}$ records the contemporaneous effect of a shock to Y_j on Y_i, and ε_t is a vector of orthogonalized disturbances with covariance matrix Σ_ε. From (12), Σ_u can be expressed in terms of B_0 and Σ_ε as

$$\Sigma_u \;=\; (I - B_0)^{-1} \Sigma_\varepsilon (I - B_0)^{-1'} \tag{13}$$

Equations (11) and (12) can be re-written with both contemporaneous and lagged effects as

$$Y_t = B_0 Y_t + \sum_{k=1}^{p} B_k \, Y_{t-k} - \sum_{k=1}^{p} B_0 B_k \, Y_{t-k} + \varepsilon_t \tag{14}$$

where B_0 models the direct contemporaneous relationships in Y_t, B_k captures the direct temporal effects at lag k, and $B_0 B_k$ summarizes the indirect lagged effect via contemporaneous channels. Equation (14) is the structural VAR model, while (11) is the reduced-form VAR designed for forecasting out-of-sample observations of multiple time series. Model (12) is a Structural Equation Model of the contemporaneous dependence among the VAR residuals. Within the VAR formulation, the matrix $B = (B_0, B_{1:p})$, is of crucial importance to understand the channels of dependence among elements in Y_t.

3.2. A Network VAR-RSEM Model

The introduction of networks in VAR models helps to interpret the serial, temporal and contemporaneous relationships in a multivariate time series. Equations (11) and (12) can be specified through networks by assigning to each coefficient $B = (B_0, B_{1:p})$ a latent indicator $G_{i,j} \in \{0, 1\}$, such that for $i, j = 1, \ldots, n$, and $l = 0, 1, \ldots, p$:

$$B_{i,j|l} = \begin{cases} 0 & \text{if} \quad G_{i,j|l} = 0 \quad \Longrightarrow \quad Y_{j,t-l} \not\rightarrow \; Y_{i,t} \\ b_{ijl} \in \mathbb{R} & \text{if} \quad G_{i,j|l} = 1 \quad \Longrightarrow \quad Y_{j,t-l} \rightarrow \; Y_{i,t} \end{cases} \tag{15}$$

where $Y_{j,t-l} \not\rightarrow Y_{i,t}$ means that Y_j does not influence Y_i at lag l, including $l = 0$, which correspond to contemporaneous dependence. Following (11), (12) and (15), a network VAR model is specified by the parameters $(p, G, B, \Sigma_\varepsilon)$, where G is related to the latent network structure, B specifies the coefficients, and Σ_ε is the residual covariance matrix.

Let $B^* = B_0 + \sum_{k=1}^{p} B_k$ and $G^* = G_0 + \sum_{k=1}^{p} G_k$. Following (15), we define two zero diagonal matrices $A \in \{0,1\}^{n\times n}$ and $A^w \in \mathbb{R}^{n\times n}$, whose ij-th element is given by:

$$A_{ij} = \begin{cases} 0, & \text{if } G^*_{i,j} = 0 \\ 1, & \text{otherwise} \end{cases}, \qquad A^w_{ij} = \begin{cases} 0, & \text{if } B^*_{i,j} = 0 \\ B^*_{i,j} & \text{otherwise} \end{cases} \tag{16}$$

where A_{ij} specifies that $Y_j \to Y_j$ exist if there is a contemporaneous or lagged directed link from Y_j to Y_i. A^w_{ij} specifies the weights of such a relationship obtained as a sum of the estimated contemporaneous and lagged coefficients. The correspondence between (G, B) and (A, A^w) is such that the former captures the short-run dynamics in Y_t while the latter can be viewed as long-term direct relationships when $Y_t = Y_{t-1} = \ldots = Y_{t-p}$. Defining a sparse structure on (G, B) induces parsimony of the short-run model and sparsity on the long-run relationship matrices (A, A^w).

The available literature on financial networks is typically focused either on structural learning or on quantitative learning. In the former case, it insists on learning G and deriving summary centrality measures, as in the work of (Battiston et al., 2012; Giudici and Spelta, 2016). In the latter case, it insists on learning B and drawing inferences from it (Billio et al., 2012; Diebold and Yilmaz, 2014). The two approaches seem not to overlap except for Ahelegbey et al. (2016a,b); Corander and Villani (2006); George et al. (2008). The proposed Network VAR-RSEM models follow the spirit of the latter.

In the next section, we introduce the model estimation framework necessary to estimate all parameters of a network VAR-RSEM model.

3.3. Bayesian Graphical Network Model Estimation

The objective of network model is to estimate (A, A^w) from $(p, G, B, \Sigma_\varepsilon)$ using the available data. Estimating these parameters jointly is a challenging problem and a computationally intensive exercise. We complete the Bayesian formulation with prior specification and posterior approximations to draw inference on the model parameters.

3.3.1. Prior Specification

We specify the prior distributions as follows:

$$p \sim \mathcal{U}(\underline{p}, \bar{p}), \qquad [B_{i,j}|G_{i,j} = 1] \sim \mathcal{N}(0, \eta), \qquad G_{i,j} \sim \text{Ber}(\pi_{ij}), \qquad \Sigma_\varepsilon^{-1} \sim \mathcal{W}(\delta, S_0)$$

where $\underline{p}$, $\bar{p}, \eta, \pi_{ij}, \delta$, and S_0 are hyper-parameters. The specification for p is a discrete uniform prior on the set $\{\underline{p}, \ldots, \bar{p}\}$, $\underline{p} < \bar{p}$.

The specification for $B_{i,j}$ conditional on $G_{i,j}$ follows a normal distribution with zero mean and variance η. Thus, relevant explanatory variables that predict a response variable must be associated with coefficients different from zero and the rest (representing not-relevant variables) are restricted to zero. We consider $G_{i,j}$ as Bernoulli distributed with π_{ij} as the prior probability. Closely related to our specification for B and G is the stochastic search variables selection (SSVS, George et al., 2008) that assumes an indicator matrix underlying B and employs the spike and slab prior on the elements in B. The SSVS and the Bayesian graphical VAR (BGVAR, Ahelegbey et al., 2016a) have proved efficient in selecting relevant variables in over-parameterized VAR models. The difference between the two methods is that the estimated SSVS coefficient matrix often consists of elements with values significantly different from zero, whereas the rest concentrate around zero but are not ignored. Parsimony is, therefore, not guaranteed.

We assume Σ_ε^{-1} is Wishart distributed with prior expectation $\frac{1}{\delta}S_0$ and $\delta > n$ the degrees of freedom parameter.

We also set $\pi_{ij} = 0.5$ which leads to a uniform prior on the graph space, i.e., $P(G_{0:p}) \propto 1$. Following standard applications, we set $\eta = 100, \delta = n + 2$ and $S_0 = \delta I_n$.

3.3.2. Posterior Approximation

Let $Z_t = (Y'_{t-1}, \ldots, Y'_{t-p})'$ be an $np \times 1$ vector of lagged observations, denote with $Y = (Y_1, \ldots, Y_N)$ a $N \times n$ matrix collection of all observations, and $Z = (Z_1, \ldots, Z_N)$ be an $N \times np$ matrix collection of lagged observations. We determine p via a Bayesian information criterion (BIC). For some lag order $\hat{p}$, the Bayesian framework of Geiger and Heckerman (2002) can be applied to integrate out the structural parameters analytically to obtain a marginal likelihood function over graphs. This allows us to apply an efficient Gibbs sampling algorithm to sample the graph structure in blocks (as in Roberts and Sahu, 1997). We approximate the graph and the parameters posterior distribution via a collapsed Gibbs sampler such that for some $\hat{p}$, the algorithm proceeds as follows:

1. Sample via a Metropolis-within-Gibbs $[G_0, G_{1:\hat{p}}|Y, \hat{p}]$ by
   (a) Sampling from the marginal distribution: $[G_{1:\hat{p}}|Y, \hat{p}]$
   (b) Sampling from the conditional distribution: $[G_0|Y, \hat{p}, G_{1:\hat{p}}]$
2. Sample from $[B_0, B_{1:\hat{p}}, \Sigma_\varepsilon|Y, \hat{G}_0, \hat{G}_{1:\hat{p}}, \hat{p}]$ by iterating the following steps:
   (a) Sample $[B_{i,\pi_i|1:\hat{p}}|Y, \hat{G}_{1:\hat{p}}, \hat{G}_0, B_0, \Sigma_\varepsilon] \sim \mathcal{N}(\hat{B}_{i,\pi_i|1:\hat{p}},\ D_{\pi_i})$ where

$$\hat{B}_{i,\pi_i|1:\hat{p}} = \sigma_{u,i}^{-2} D_{\pi_i} Z'_{\pi_i} Y_i, \qquad D_{\pi_i} = (\eta^{-1} I_{d_z} + \sigma_{u,i}^{-2} Z'_{\pi_i} Z_{\pi_i})^{-1} \tag{17}$$

   where $Z_{\pi_i} \in Z$ which corresponds to $(\hat{G}_{y_i, z_\pi|1:\hat{p}} = 1)$, $\sigma_{u,i}^2$ is the i-th diagonal element of $\hat{\Sigma}_u = (I - \hat{B}_0)^{-1}\hat{\Sigma}_\varepsilon (I - \hat{B}_0)^{-1'}$, and d_z is the number of covariates in Z_{π_i}.
   (b) Sample $[B_{i,\pi_i|0}|Y, \hat{G}_0, \hat{G}_{1:\hat{p}}, B_{1:\hat{p}}, \Sigma_\varepsilon] \sim \mathcal{N}(\hat{B}_{i,\pi_i|0}, Q_{\pi_i})$ where

$$\hat{B}_{i,\pi_i|0} = \sigma_{\varepsilon,i}^{-2} Q_{\pi_i} \hat{U}'_{\pi_i} \hat{U}_i, \qquad Q_{\pi_i} = (\eta^{-1} I_{d_u} + \sigma_{\varepsilon,i}^{-2} \hat{U}'_{\pi_i} \hat{U}_{\pi_i})^{-1} \tag{18}$$

   where $\hat{U} = Y - Z\hat{B}'_{1:\hat{p}}$, $\hat{U}_{\pi_i} \in \hat{U}_{-i}$ is the set of contemporaneous predictors of $\hat{U}_i$ that corresponds to $(\hat{G}_{y_i, y_\pi|0} = 1)$, and d_u is the number of covariates in U_{π_i}
   (c) Sample $[\Sigma_\varepsilon^{-1}|Y, \hat{G}_{1:\hat{p}}, \hat{G}_0, B_{1:\hat{p}}, B_0] \sim \mathcal{W}(\delta + N,\ S_N)$ where

$$S_N = S_0 + (\hat{U} - \hat{U}\hat{B}'_0)'(\hat{U} - \hat{U}\hat{B}'_0) \tag{19}$$

Sampling $[G_0, G_{1:\hat{p}}]$ jointly is a computationally intensive exercise. For instance, the number of possible networks of temporal dependence in a VAR of n variables with p lags is 2^{pn^2}, and the number of possible contemporaneous dependencies that allows for simultaneity is $2^{n(n-1)}$. Therefore sampling $[G_0, G_{1:\hat{p}}]$ jointly means searching for a single best network in a space with $2^{pn^2+n(n-1)}$ possible structures. We, instead, sample from $[G_0, G_{1:\hat{p}}|Y, \hat{p}]$ by modifying the algorithm in Ahelegbey et al. (2016a). More precisely, we sample $G_{1:\hat{p}}$ from its marginal distribution and G_0 from a conditional distribution. A detailed description of the network sampling algorithm and convergence diagnostics in Appendix A.

4. Data Description

The data we consider to illustrate our methodology is taken from the Bloomberg database and consists of the daily market indices of 20 countries, selected according to their market capitalization. We consider only one index per country, which typically contains the stock prices of the largest companies listed in the nation's largest stock exchange. The considered countries can be grouped into three regions: the Americas (Brazil, Canada, Mexico, and the United States), Asia-Pacific (Australia, China, Hong Kong, India, Japan, and South Korea), and Europe (Belgium, France, Germany, Italy, the Netherlands, Portugal, Russia, Spain, Switzerland, and the United Kingdom). A description of the market indices chosen for the selected countries is presented in Table 1. The data cover January 3, 2000, to June 30, 2020.

Region	No.	Country	Code	Description	Index
Americas	1	Brazil	BR	Brazil Bovespa	IBOV
	2	Canada	CA	Canada TSX Comp.	SPTSX
	3	Mexico	MX	Mexico IPC	MEXBOL
	4	United States	US	United States S&P 500	SPX
Asia-Pacific	5	Australia	AU	Australia ASX 200	AS51
	6	China	CN	China SSE Comp.	SHCOMP
	7	Hong Kong	HK	Hong Kong Hang Seng	HSI
	8	India	IN	India BSE Sensex	SENSEX
	9	Japan	JP	Japan Nikkei 225	NKY
	10	Korea	KR	South Korean KOSPI	KOSPI
Europe	11	Belgium	BE	Belgium BEL 20	BEL20
	12	France	FR	France CAC 40	CAC
	13	Germany	DE	Germany DAX 30	DAX
	14	Italy	IT	Italy FTSE MIB	FTSEMIB
	15	Netherlands	NL	Netherlands AEX	AEX
	16	Portugal	PT	Portugal PSI 20	PSI20
	17	Russia	RU	Russia MOEX	IMOEX
	18	Spain	ES	Spain IBEX 35	IBEX
	19	Switzerland	CH	Switzerland SMI	SMI
	20	United Kingdom	UK	UK FTSE 100	UKX

Table 1: Detailed description of stock market indices of countries classified according to regions.

The selected market indices vary in terms of composition, in the sense that some have a smaller number of stocks compared to others. For instance, the U.S. is represented by the S&P 500, which contains the stocks of the top 500 large-cap corporations, whereas France is represented by CAC 40, which contains 40 stocks selected among the top 100 corporations.

Figure 1 reports the plot of daily closing prices on a logarithmic scale. Due to differences in the values, plotting the original prices would be difficult to visualize. We, therefore, scale the prices to a zero mean and unit variance and add the absolute minimum value of each series to avoid negative outcomes. This standardizes the scale of measurement for the different series. Figure 1 clearly shows that, amid many fluctuations, and some local specificities, stock market indices are highly synchronized and have been affected by three major downturns: 2000–2003 period (the tech-bubble crisis); 2007–2009 (sub-prime and global financial crisis); and the 2020 (COVID-19 pandemic). To help the interpretation of these sub-periods, Table 2 reports a summary description of the main events recorded during the major downturns.

Figure 1 and Table 2 show that financial markets are initially slow to adjust to the

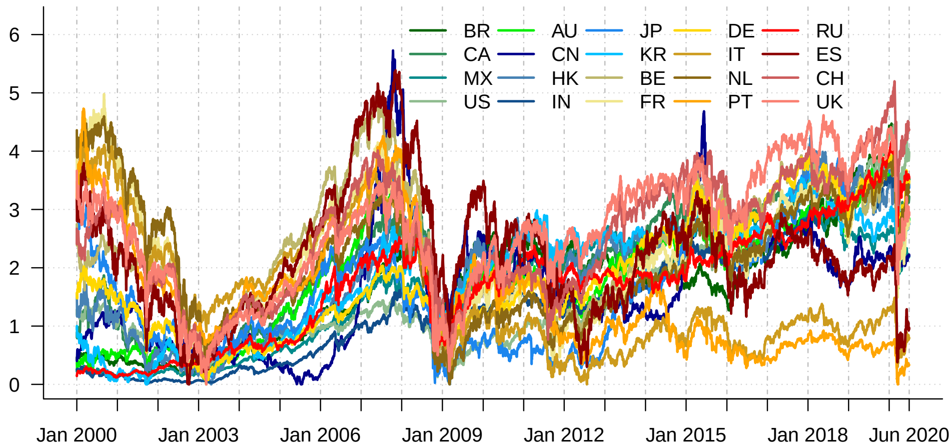

Figure 1: Time series of daily stock market prices on a logarithmic scale (January 3, 2000 – June 30, 2020).

	Dates	Event Details
1	Mar 10, 2000 – Mar 12, 2003	Collapse of Dot-com bubble (Mar 10, 2000) Decline in economic activity after Sept 11, 2001 Stock market downturn of Oct 9, 2002
2	Oct 11, 2007 – Mar 9, 2009	Fall in housing prices that peaked in Oct 2007 Near-collapse and acquisition of Bear Sterns in Mar 2008 Bankruptcy of Lehman Brothers & bailout of AIG in Sep 2008
3	Feb 24, 2020 –	COVID-19 outbreak in China in late 2019 began to affect Europe and the U.S., plunging many stock markets into turmoil.

Table 2: Stock market large downturns between January 2000 – June 2020.

emergence of a crisis. They, however, tend to over-react as the crises begin to spread and affect different markets through interconnectedness. Although there is not yet much data to fully compare the COVID-19 crisis with the previous tech and sub-prime crisis, the daily plunge in prices between February 24, 2020, and June 30, 2020, as illustrated in Figure 1 provides evidence that the market decline occurs simultaneously for all the three periods.

Tensions in equity markets can be analyzed via stock market prices/returns with a huge drop in price implying a rise in financial stress. We report in Table 3 the dates of historical high financial stress in the world 20 major stock markets across the three major financial crisis periods: (2000–2003), (2007–2009), and (2020:H1). This comparison helps to understand the peculiarity of the different crises. We notice from the table that, during the tech crisis, the largest daily drop in the US S&P 500 was 5.83 percent, recorded on April 14, 2000; during the sub-prime crisis it was 9.03%, on October 15, 2008; and 11.98% on March 16, 2020, during the COVID-19 outbreak. Indeed, Table 3 suggests that, compared with other crises, the COVID-19 pandemic is having an unprecedented impact on the world's major equity markets, with 13 out of the top 20 national stock market indices recording their maximum daily downturn of the 21st century occurring in March 2020.

Country	2000 – 2003	2007 – 2009	2020
Brazil	9.18 : 2001-09-11	11.39 : 2008-10-15	**14.78** : 2020-03-12
Canada	8.12 : 2000-10-25	9.32 : 2008-12-01	**12.34** : 2020-03-12
Mexico	**7.93** : 2000-04-14	7.01 : 2008-10-22	6.42 : 2020-03-09
United States	5.83 : 2000-04-14	9.03 : 2008-10-15	**11.98** : 2020-03-16
Australia	5.40 : 2000-04-17	8.34 : 2008-10-10	**9.70** : 2020-03-16
China	6.33 : 2002-01-28	**8.84** : 2007-02-27	3.86 : 2020-01-28
Hong Kong	8.87 : 2001-09-12	**12.7** : 2008-10-27	4.86 : 2020-03-23
India	7.15 : 2000-04-04	10.96 : 2008-10-24	**13.15** : 2020-03-23
Japan	6.98 : 2000-04-17	**11.41** : 2008-10-16	6.08 : 2020-03-13
Korea	**12.02** : 2001-09-12	10.57 : 2008-10-24	8.39 : 2020-03-19
Belgium	5.46 : 2001-09-11	7.98 : 2008-09-29	**14.21** : 2020-03-12
France	7.39 : 2001-09-11	9.04 : 2008-10-06	**12.28** : 2020-03-12
Germany	8.49 : 2001-09-11	7.16 : 2008-01-21	**12.24** : 2020-03-12
Italy	7.57 : 2001-09-11	8.24 : 2008-10-06	**16.92** : 2020-03-12
Netherlands	7.25 : 2001-09-14	9.14 : 2008-10-06	**10.75** : 2020-03-12
Portugal	4.46 : 2001-09-11	**9.86** : 2008-10-06	9.76 : 2020-03-12
Russia	9.95 : 2003-10-30	**18.66** : 2008-10-06	8.28 : 2020-03-12
Spain	5.82 : 2001-09-14	9.14 : 2008-10-10	**14.06** : 2020-03-12
Switzerland	7.07 : 2001-09-11	7.79 : 2008-10-10	**9.64** : 2020-03-12
United Kingdom	5.72 : 2001-09-11	8.85 : 2008-10-10	**10.87** : 2020-03-12

Table 3: Dates of historical high financial stress in major stocks markets over the periods: (2000–2003), (2007–2009), and (2020:H1). Bold values indicate the maximum drop of each index over the three crisis periods.

5. Empirical Findings

We apply our proposed methodology to study the interconnectedness among the major financial markets. We compute daily returns as the log differences of successive daily closing prices. We obtain monthly estimates of the model parameters and construct the matrices Ω and S_σ, which are the core components of our network-based turbulence score. To improve the efficiency of the estimates of Ω we aggregate monthly estimates in yearly rolling windows of about 240 trading days. We set the increments between successive rolling windows to one month, setting the first window of our study from February 1, 1999, to January 31, 2000, followed by March 1, 1999, to February 29, 2000; the last window is from July 1, 2019, to June 30, 2020. In total, we consider 246 rolling windows. To avoid over smoothing, S_σ is instead estimated monthly, that is, using only the last month of each rolling window.

We select the appropriate lag of the VAR via a Bayesian information criterion (BIC) for different lag orders ($p \in \{1, \ldots, 7\}$). Table 4 presents the BIC scores corresponding to the different lag orders. The minimum BIC score, which indicates the optimal lag order, is represented in boldface. Thus, we conduct our rolling estimations using a lag order of $p = 1$.

	p=1	p=2	p=3	p=4	p=5	p=6	p=7
BIC	**-17.22**	-16.85	-16.42	-15.96	-15.50	-15.02	-14.54

Table 4: The BIC scores for lag order selection of the VAR model. Boldface values indicate the minimum BIC.

We present our main findings in line with answering the following research questions:

RQ-1 Does a densely interconnected market reduce or amplify financial risks?

RQ-2 Is there a threshold of risk beyond which financial connections serves as shock-amplifiers?

RQ-3 Which major world market is central to the creation of global financial market risk?

We answer RQ-1 by studying the relationship between Net-Density, NetVIX, and the VIX[1] in Section 5.1. We report the relationship between the NetVIX and the VIX in Section 5.2. We monitor the AVX and NetX to identify the threshold of risks beyond which dense connections serve as shock-amplifiers, answering RQ-2, in Section 5.3. Finally, we study the marginal volatility indices (MVX_i) to identify the highest risk-contributing markets central to the creation of global meltdown, thus answering RQ-3, in Section 5.4.

5.1. Relationship Between Net-Density, NetVIX and VIX

Here we address our first research question: (RQ-1) Does a densely interconnected network reduce or amplify the financial risks caused by shock events?

We report in Figure 2 the plot of Net-Density, NetVIX, and VIX. The figure shows a striking resemblance between the NetVIX and VIX, both proving a similar signal about the "direction" of global market risk. Both indices indicate spikes during the tech-bubble crisis (2000–2003), the global financial crisis (GFC, 2007–2009), the Eurozone crisis (2010–2013), the Chinese stock market turbulence (2015–2016), and the recent Covid-19 pandemic (2020:1H). The historical highest spike recorded for the COVID is only second to that of the GFC, which indicates evidence of strong contagion in the equities market during the GFC and the COVID pandemic, more than in the tech-bubble and Eurozone crisis. We notice that periods of historic spikes in the NetVIX and VIX are associated with a higher degree of interconnectedness as depicted by Net-Density. In particular, the degree of interconnectedness recorded for the COVID seems to have reached the same height as that of the GFC, suggesting that the behavior of the stock markets during the pandemic is in several ways more similar to the GFC than it is to other periods of financial stress.

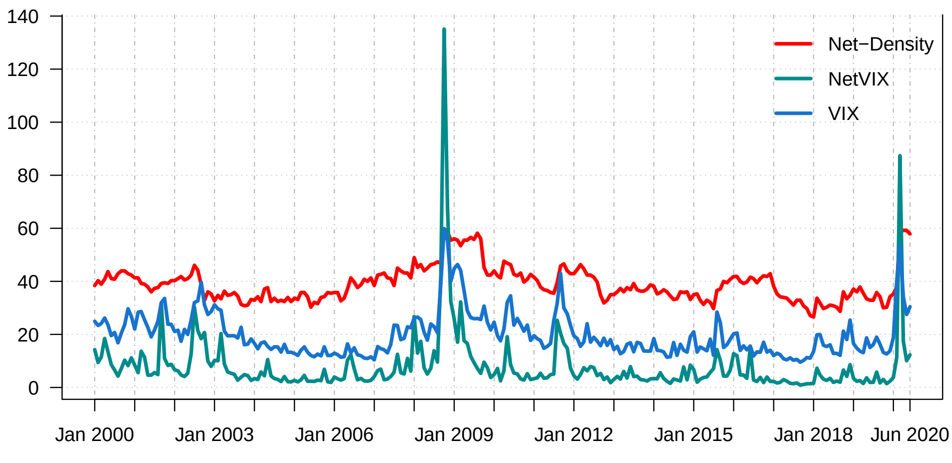

Figure 2: Historic monthly series of Net-Density, NetVIX and VIX (January 2000 – June 2020).

We notice a slight difference between the NetVIX and VIX. That is, although the VIX is consistently higher than the NetVIX most of the time, the latter reports higher values of risk especially in the GFC and COVID periods. This suggests that the computation of the VIX may include a smoothing effect that lowers the predicted market risk in times of crisis.

[1]The VIX reflects the market's expectation of volatility based on the S&P 500 index.

	Min	Median	Mean	Max	St. Dev.	Q0.25	Q0.75
Net-Density	26.5789	37.8947	39.0116	59.7368	6.5773	34.2105	42.3026
NetVIX	0.8985	4.7167	7.9544	135.0996	12.1002	2.9736	8.5413
VIX	9.5100	17.5300	19.8474	59.8900	8.2825	13.7950	23.6450

Table 5: Summary statistics of Net-Density, NetVIX and VIX (January 2000 – June 2020).

We report in Table 5 the summary statistics of the three indices. The table shows that the Net-Density, NetVIX, and VIX average around 39, 7.95, and 19.85, with a standard deviation of 6.58, 12.1, and 8.28, respectively. The Net-Density is range-bound between 26.58 to 59.7. The all-time monthly low for the NetVIX and VIX is 0.9 and 9.5, while the all-time monthly high is around 135.1 and 59.9, respectively.

In the interest of analyzing the relationship between dense financial interconnectedness and global market risk, we study the lead-lag relationship between the pairs (Net-Density and NetVIX), and (Net-Density and VIX). We stationarize each series via first differencing. Table 6 presents the results of the cross-correlation of the first difference of Net-Density with NetVIX and VIX. The table shows that the highest cross-correlation between the Net-Density

	Cross-correlation of ΔNet-Density(t) with										
x_{t+h}	-5	-4	-3	-2	-1	0	1	2	3	4	5
ΔNetVIX	-0.02	-0.04	-0.01	-0.08	-0.29	**0.46**	0.13	-0.06	-0.04	0.01	-0.03
ΔVIX	-0.03	-0.04	-0.01	-0.07	-0.13	**0.33**	0.24	-0.01	-0.04	-0.03	-0.01

Table 6: Cross-correlation of Net-Density with NetVIX and NetVIX. The result shows the correlation of x_{t+h} (the row variable) with y_t (the column variable). Boldface values indicate the significant correlations.

and NetVIX and between the Net-Density and VIX all occurs at lag 0, suggesting evidence of a significant positive contemporaneous relationships. We model the relationship between the pairs via an autoregression, moving averages and integration (ARIMA) framework:

$$\Delta DV_t = \beta\ \Delta Net.D_t + \Phi_1 \Delta DV_{t-1} + \Theta_1 \xi_{t-1} + \xi_t \tag{20}$$

$$\Delta DV_t = \Phi_1 \Delta DV_{t-1} + \Theta_1 \xi_{t-1} + \xi_t \tag{21}$$

where $Net.D_t$ is the Net-Density at time t, DV_t is either VIX or NetVIX, ξ_t is the error term.

	VIX		NetVIX	
	ARIMAX(1,1,1)	ARIMA(1,1,1)	ARIMAX(1,1,1)	ARIMA(1,1,1)
Φ_1	0.5800***	0.5544***	0.4428***	0.4902***
Θ_1	-1.0000***	-0.8466***	-1.0000***	-0.9295***
β	0.5612***		0.3519***	
σ^2	11.5665	62.9099	81.0975	106.5521
AIC	1,307.2590	1,716.3580	1,784.7750	1,846.1490

Table 7: Impact of Net-Density on VIX and NetVIX. Note: *** indicates are 1% level of significance.

Given that we are interested in the relationship between dense stock market interconnectedness and global market risk, we condition the above ARIMA framework on periods with top

25% Net-Density. We use the above equations to test the effect of Net-Density on the NetVIX and VIX. If β is significantly different from zero then $Net.D$ affects DV. Alternatively, if the covariance of the residuals from (20) is smaller than that of (21), then $Net.D$ affects DV.

The result presented in Table 7 shows that the β-coefficients are positive and statistically significant, which indicates that periods of dense stock market interconnectedness increases global market risk. This is in line with the findings of Billio et al. (2012) and Blume et al. (2013), among others, for which dense interconnectedness does amplify financial market risk.

5.2. Relationship Between NetVIX and VIX

We present in Table 8 the cross-correlation of the first difference of VIX with NetVIX. The table reports the highest cross-correlation occurring at lag 0, which suggests evidence of a strong positive contemporaneous relationship.

	Cross-correlation of ΔVIX(t) with								
x_{t+h}	-4	-3	-2	-1	0	1	2	3	4
ΔNetVIX	0.024	0.016	-0.247	0.042	**0.580**	0.123	-0.265	-0.135	0.006

Table 8: Cross-correlation of VIX with NetVIX. The result shows the correlation of x_{t+h} (the row variable) with y_t (the column variable). Boldface values indicate the significant correlations.

We model the marginal distribution of the NetVIX as ARIMA(1,1,1) and the conditional distribution of the VIX given NetVIX as ARIMAX(2,1,1).

$$\Delta NetVIX_t = \Phi_1 \Delta NetVIX_{t-1} + \Theta_1 \xi_{t-1} + \xi_t \tag{22}$$
$$\Delta VIX_t = \beta \ \Delta NetVIX_t + \Phi_1 \Delta VIX_{t-1} + \Phi_2 \Delta VIX_{t-2} + \Theta_1 \xi_{t-1} + \xi_t \tag{23}$$
$$\Delta VIX_t = \Phi_1 \Delta VIX_{t-1} + \Theta_1 \xi_{t-1} + \xi_t \tag{24}$$

where (22) is the ARIMA(1,1,1) NetVIX model, (23) is the ARIMAX(2,1,1) VIX model with the NetVIX as an exogenous variable, and (24) is the ARIMA(1,1,1) VIX benchmark model. The result is shown in Table 9[2]. The table confirms the significant contemporaneous impact

	NetVIX	VIX	
	ARIMA(1,1,1)	ARIMAX(1,1,1)	ARIMA(1,1,1)
Φ_1	0.5547***	0.4690***	0.7601***
Φ_2		0.2008**	
Θ_1	-0.9999***	-0.8949***	-0.9328***
β		0.3078***	
σ^2	102.0953	13.2295	21.4432
AIC	1,838.8690	1,338.3600	1,452.7390
RMSE	10.0837	3.6298	4.6213

Table 9: Impact of NetVIX on VIX. Note: ***, **, and * are 1%, 5% and 10% level of significance respectively.

of the NetVIX on the VIX. Table 10 presents the out-of-sample forecast of the monthly VIX for the rest of the year 2020 compared with the realized values for the months of July–August 2020[3]. The results indicate that not only does the ARIMAX(2,1,1) performs better than the

[2]We conduct model diagnostics to ensure there is no serial correlation and heteroscedasticity in residuals.

[3]We forecast out-of-sample NetVIX which are then used for predicting the VIX via ARIMAX(2,1,1).

	Realized (VIX)	Forecast (VIX)	
		ARIMAX(2,1,1)	ARIMA(1,1,1)
2020-07	24.4600	27.9478	28.8076
2020-08	26.4100	27.1818	27.5744
2020-09		26.4143	26.6371
2020-10		25.9505	25.9247
2020-11		25.6066	25.3832
2020-12		25.3676	24.9716

Table 10: Out-of-sample point forecast of VIX according to ARIMAX(2,1,1) and ARIMA(1,1,1).

benchmark - ARIMAX(1,1,1) in terms of the RMSE of the in-sample training set, but also the out-sample forecasts are much closer to the realized observation than the benchmark. In summary, we document evidence of a significant relationship between the NetVIX and VIX, with both indices providing similar signals about the direction of global market risk. In addition, the NetVIX improves the prediction of the VIX.

5.3. Global Stage Decomposition of NetVIX

We now turn our attention to the second research question: (RQ-2) Is there a threshold of risks beyond which financial interconnectedness serves as shock-amplifiers?

We address this question by studying the NetX and AVX and the volatility of some selected market indices like the US S&P-500 (SPX), Germany DAX-30 (DAX), France CAC-40 (CAC), Hong Kong Hang Seng (HSI), and Japan Nikkei-225 (NKY). Figure 3 plots the monthly series of these indices over the sample period. We quickly notice some similarity between Figure 3 and Figure 2. That is, the dynamics in the AVX and the volatilities of S&P-500, DAX-30, CAC-40, HangSeng, and Nikkei follow that of the NetVIX and VIX.

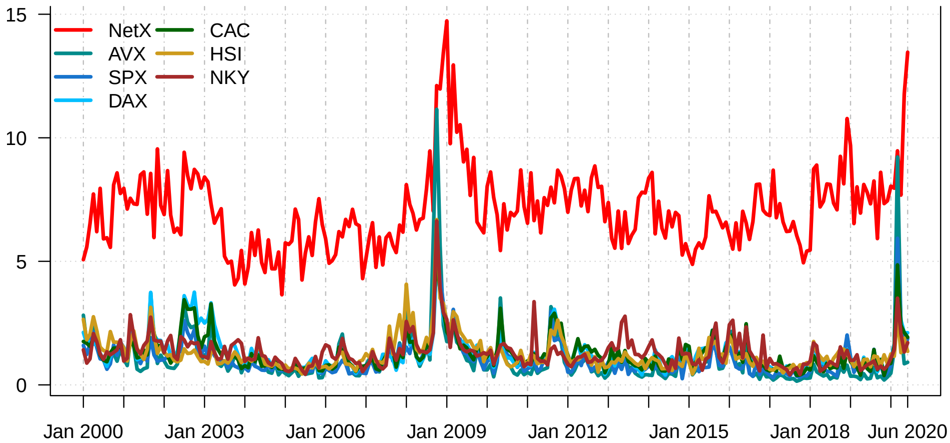

Figure 3: Monthly series of NetX, AVX and volatilities of S&P-500, DAX-30, CAC-40, HangSeng and Nikkei.

Table 11 reports the summary statistics of these indices. The table shows that over the last two decades, the volatilities of these major market indices ranged from 0.25 (S&P 500 - SPX) to 6.69 (Hang Seng - HSI) with historical averages around (1.04–1.32). The AVX and NetX, over the period, ranges between 0.719–11.154 and 3.65–14.7, with a historic mean of 1.04 and 7. This suggests that on average, stock market interconnectedness amplifies the average market volatility by 700 percent to create global market risk. During turbulent times (measured by Q0.75), the weighted average stock market risk is around 1.16 (1.2 for S&P 500, 1.56 for Nikkei 225), and the NetX is around 7.96 which confirms the initial results that a higher degree of stock market interconnectedness does amplify market risks.

	Min	Median	Mean	Max	St. Dev	Q0.25	Q0.75
NetX	3.6471	6.9113	7.0668	14.7316	1.6490	5.9874	7.9591
AVX	0.1486	0.7190	1.0419	11.1540	1.1634	0.4593	1.1554
SPX(σ)	0.2517	0.8716	1.0402	5.9332	0.7159	0.5850	1.2069
DAX(σ)	0.3874	1.1074	1.3093	4.9133	0.7260	0.8040	1.5316
CAC(σ)	0.3752	1.1069	1.2762	5.1675	0.7132	0.7784	1.5238
HSI(σ)	0.4359	1.0933	1.2679	6.6912	0.6912	0.8555	1.4423
NKY(σ)	0.4081	1.2045	1.3202	6.6367	0.6565	0.9185	1.5555

Table 11: Statistics of NetX, AVX and volatilities of S&P-500, DAX-30, CAC-40, HangSeng and Nikkei.

A careful look at the plot in Figure 3 shows that AVX precedes NetX by some lags. To verify this claim, we perform the cross-correlation test of the first difference in NetX with the volatility measures conditional on the top 25% NetX periods. Table 12 shows that periods of top 25% NetX are preceded by higher AVX as evidenced by the significant cross-correlation coefficient between the first difference of NetX and AVX at lag 1.

	Cross-correlation of ΔNetX(t) with								
x_{t+h}	-4	-3	-2	-1	0	1	2	3	4
ΔAVX	0.008	0.066	0.096	0.000	0.249	**-0.288**	-0.036	-0.097	0.050
ΔSPX(σ)	0.030	0.005	0.071	-0.001	**0.363**	-0.211	-0.037	-0.102	0.026
ΔDAX(σ)	0.067	-0.052	0.086	-0.046	**0.398**	-0.242	-0.077	-0.102	0.064
ΔCAC(σ)	0.051	0.008	0.074	0.020	**0.308**	-0.270	-0.065	-0.111	0.032
ΔHSI(σ)	-0.087	0.076	0.086	-0.028	**0.427**	**-0.393**	0.119	-0.105	0.004
ΔNKY(σ)	-0.238	0.088	0.184	-0.099	**0.488**	**-0.417**	0.105	-0.105	-0.079

Table 12: Cross-correlation of NetX with AVX, volatilities of S&P-500, DAX-30, CAC-40, HangSeng and Nikkei. The result shows the correlation of x_{t+h} (the row variable) with y_t (the column variable).

In the interest of finding the threshold of stock market risks beyond which financial interconnectedness serve as shock-amplifiers, we adopt the approach of Kinlaw and Turkington (2013) by performing analysis with the following steps:

1. Identify the top 25% percent of the full sample with the highest AVX scores
2. Partition the selected times into two non-overlapping subsamples: one with high NetX scores (greater than 7) and another with low NetX score (less than or equal to 7). Note: 7 is the historical average and median NetX score.
3. Perform a two-sample t-test of the differences in mean (high NetX - low NetX)

Table 13 presents the test results for the selected markets for periods with top 25% AVX and high NetX against those with low NetX. The top panel of the table reports the contemporaneous volatility conditions for months recording the top 25% AVX with high/low NetX. The second panel reports the volatility conditions one month following these recordings. This is repeated for the third, through to six months following the periods of top 25% AVX with high/low NetX. Overall, we notice that in the months with top 25% AVX-high NetX, the average stock market risks are significantly higher than those with top 25% AVX-low NetX.

	SPX(σ)	DAX(σ)	CAC(σ)	HSI(σ)	NKY(σ)
	Contemporaneous Relationship: Same Month				
Top 25% AVX (all observation)	1.833	2.187	2.155	2.018	1.914
Top 25% AVX with NetX> 7 (x_0)	2.195	2.509	2.433	2.179	2.086
Top 25% AVX with NetX≤ 7 (x_1)	1.259	1.676	1.716	1.763	1.641
Difference in mean ($x_0 - x_1$)	0.936	0.833	0.717	0.417	0.444
p-value of Two Sample t-test	0.000	0.000	0.000	0.051	0.021
	Predicting Volatility: Following Month				
Top 25% AVX (all observation)	1.623	1.959	1.894	1.769	1.730
Top 25% AVX with NetX> 7 (x_0)	1.942	2.298	2.204	2.025	1.910
Top 25% AVX with NetX≤ 7 (x_1)	1.118	1.423	1.403	1.363	1.445
Difference in mean ($x_0 - x_1$)	0.823	0.876	0.801	0.662	0.465
p-value of Two Sample t-test	0.000	0.000	0.000	0.001	0.016
	Predicting Volatility: Following Three-Months				
Top 25% AVX (all observation)	1.341	1.651	1.563	1.581	1.536
Top 25% AVX with NetX> 7 (x_0)	1.515	1.887	1.725	1.683	1.639
Top 25% AVX with NetX≤ 7 (x_1)	1.073	1.287	1.314	1.423	1.378
Difference in mean ($x_0 - x_1$)	0.441	0.600	0.411	0.260	0.261
p-value of Two Sample t-test	0.012	0.001	0.017	0.225	0.160
	Predicting Volatility: Following Four-Months				
Top 25% AVX (all observation)	1.236	1.555	1.465	1.451	1.409
Top 25% AVX with NetX> 7 (x_0)	1.395	1.747	1.596	1.510	1.519
Top 25% AVX with NetX≤ 7 (x_1)	0.998	1.266	1.269	1.361	1.243
Difference in mean ($x_0 - x_1$)	0.397	0.480	0.328	0.149	0.276
p-value of Two Sample t-test	0.015	0.010	0.043	0.353	0.053
	Predicting Volatility: Following Five-Months				
Top 25% AVX (all observation)	1.214	1.594	1.505	1.504	1.485
Top 25% AVX with NetX> 7 (x_0)	1.341	1.791	1.637	1.608	1.548
Top 25% AVX with NetX≤ 7 (x_1)	1.029	1.307	1.313	1.353	1.394
Difference in mean ($x_0 - x_1$)	0.312	0.484	0.323	0.255	0.154
p-value of Two Sample t-test	0.058	0.004	0.046	0.188	0.296
	Predicting Volatility: Following Six-Months				
Top 25% AVX (all observation)	1.227	1.618	1.561	1.562	1.526
Top 25% AVX with NetX> 7 (x_0)	1.266	1.735	1.615	1.534	1.518
Top 25% AVX with NetX≤ 7 (x_1)	1.171	1.448	1.482	1.601	1.538
Difference in mean ($x_0 - x_1$)	0.094	0.287	0.134	-0.067	-0.019
p-value of Two Sample t-test	0.689	0.196	0.560	0.807	0.941

Table 13: Statistical test of differences in mean for periods with top 25% AVX with NetX threshold at 7.

The first month following these events also exhibits similar market volatility behaviors across the selected markets. This observation seems to persist longer in some markets than others. For instance, the persistent high market volatilities in Hong Kong (HSI) and Japan (NKY) does not go beyond one month. In the US, the persistence runs into four months, while Germany and France linger on until the fifth month.

In summary, the result shows that during turbulent times, the weighted average market volatility is usually higher than the 75th percentile mark with the associated stock market interconnectedness likely to amplify market risk more than 700 percent to cause a global meltdown. Also during crisis times, the level of average market risk is relatively higher and more persistent in some markets (like the US, Germany, and France) than others (like Hong Kong and Japan), which implies market losses for investors already with long exposures.

5.4. Local Stage Decomposition of NetVIX

We now address our third research question: (RQ-3) Which major world market is central to the creation of global financial risk?

To address this question, we first analyze the topological structure of interconnectedness among the world stock markets to assess which markets are more central and, therefore, systematically more relevant to financial market turbulence over the past first two decades. We divide the full sample into six sub-periods of tranquil (non-crisis) periods and turbulent times: (2000–2003), (2004–2006), (2007–2009), (2010–2013), (2014–2019) and 2020:1H.

We report in Figure 4 the network topology over the sub-periods. Each network is represented with color-coded links and nodes. Red-links indicate negative weights and green-links denote positive weights. Red-color nodes represent American markets, blue-nodes for European markets, and green-nodes for markets in Asia-Pacific countries. The size of the nodes is proportional to their hub scores. The figure provides strong evidence of clustering among

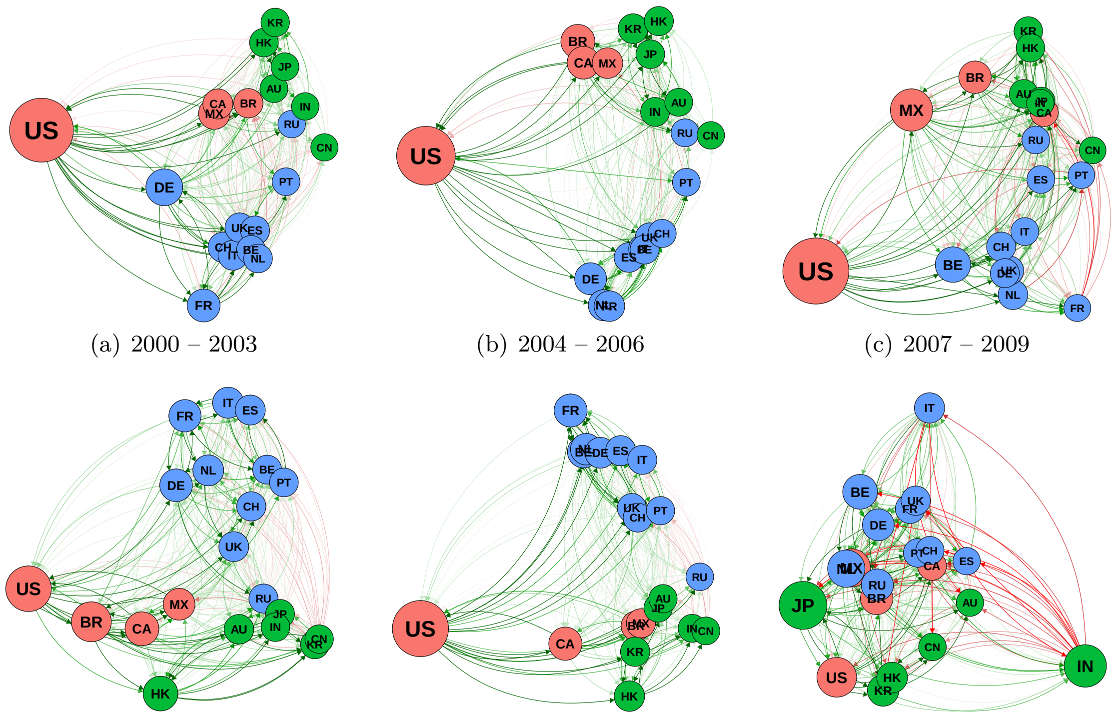

(a) 2000 – 2003 (b) 2004 – 2006 (c) 2007 – 2009

(d) 2010 – 2013 (e) 2014 – 2019 (f) 2020:1H

Figure 4: Sub-period networks. Red nodes denote markets in the Americas, blue for European countries, and green for Asia-Pacific countries. The size of the nodes are based on a weighted out-degree.

the markets. More importantly, the Asian-Pacific markets (green-nodes) seem to move together, likewise, the European markets (blue-nodes) due to similarities in underlying market conditions. The US, however, appears separated from the others most of the time, as the rest of the American markets (red-nodes) are usually closer to the Asia-Pacific ones. We notice that the US is usually the biggest sized node and strongly positively connected to the rest of

	Rank	Hub	Auth	MVX
Sub-Periods: Top Three Most Influential				
2000 – 2003	1	US (0.434)	NL (0.300)	US (1.626)
	2	DE (0.293)	FR (0.282)	DE (0.897)
	3	FR (0.269)	UK (0.268)	FR (0.740)
2004 – 2006	1	US (0.474)	FR (0.325)	US (0.940)
	2	DE (0.280)	NL (0.310)	BR (0.496)
	3	FR (0.262)	ES (0.298)	KR (0.429)
2007 – 2009	1	US (0.370)	FR (0.285)	US (1.959)
	2	MX (0.314)	ES (0.265)	MX (1.310)
	3	BE (0.251)	BE (0.259)	HK (0.836)
2010 – 2013	1	BR (0.363)	NL (0.288)	US (0.846)
	2	US (0.339)	FR (0.286)	BR (0.713)
	3	UK (0.250)	DE (0.284)	HK (0.592)
2014 – 2019	1	US (0.467)	NL (0.310)	US (0.813)
	2	BE (0.267)	BE (0.300)	HK (0.483)
	3	FR (0.261)	FR (0.298)	FR (0.460)
2020:1H	1	JP (0.349)	CA (0.260)	JP (2.186)
	2	IN (0.344)	NL (0.257)	NL (1.518)
	3	MX (0.302)	PT (0.254)	US (1.449)
Full-Sample: All Countries				
Core	1	US (0.417)	FR (0.293)	US (0.994)
	2	DE (0.254)	NL (0.292)	BR (0.551)
	3	FR (0.251)	BE (0.272)	HK (0.524)
	4	NL (0.237)	DE (0.269)	FR (0.505)
	5	BE (0.232)	UK (0.267)	DE (0.483)
Semi-Periphery	6	IT (0.218)	CH (0.257)	ES (0.434)
	7	CH (0.217)	IT (0.251)	CA (0.433)
	8	UK (0.210)	ES (0.248)	MX (0.432)
	9	ES (0.205)	PT (0.207)	IT (0.420)
	10	BR (0.203)	HK (0.204)	BE (0.418)
	11	CA (0.171)	JP (0.200)	NL (0.416)
	12	KR (0.157)	AU (0.194)	KR (0.385)
	13	HK (0.152)	RU (0.192)	JP (0.347)
	14	MX (0.148)	KR (0.190)	UK (0.346)
	15	RU (0.144)	US (0.169)	RU (0.313)
Periphery	16	PT (0.135)	BR (0.166)	CH (0.292)
	17	JP (0.131)	CA (0.164)	AU (0.289)
	18	IN (0.110)	IN (0.159)	PT (0.278)
	19	CN (0.102)	MX (0.157)	IN (0.260)
	20	AU (0.090)	CN (0.102)	CN (0.183)

Table 14: Centrality ranking of markets according to hub, authority and marginal VIX scores.

the markets. Based on the node sizes, the US appears to be the most influential in almost all the sub-periods except 2020-1H, where Japan seems to dominate.

Table 14 reports the centrality of the markets based on the median hub, authority, and marginal VIX scores. The table shows the top three ranked markets for the sub-periods, and the full sample ranking from "core" (1st to 5th), through "semi-periphery" (6th to 15th), to "periphery" (16th to 20th). Over the last two decades, the US is by far the most dominant market in terms of spillover propagation based on hub score ranking. It is usually within the top three highest hub-score markets, except for 2020:1H. It is followed by Germany, France, the Netherlands, and Belgium. Indeed, these European markets are integrated in Euronext - a unique marketplace connecting many European economies. Thus, spillover in stock markets propagates from the US and EU-centered markets, like Germany and France.

The authority score centrality shows the most affected markets are France, the Netherlands, Belgium, Germany, and the UK. Again, these are European markets, which implies that the markets most affected by spillover propagation are mainly European-centered markets.

Finally, the marginal VIX score centrality shows that the highest contributors to global market turbulence are the US, Brazil, Hong Kong, France, and Germany. At the bottom is Mainland China with the lowest marginal VIX score. This suggests that financial market participants must carefully track events in these markets.

Overall, we observe that although spillovers in stock markets propagate from the US, Germany, France, the Netherlands, and Belgium to other markets, the highest risk-contributing markets to global meltdown are the US, Brazil, Hong Kong, France, and Germany. The inclusion of Brazil and Hong Kong in the top global risk contributors confirm the importance of analyzing the state and direction of financial markets via our NetVIX measure.

6. Conclusion

We construct a network volatility index (NetVIX) that incorporates market interconnectedness and volatilities to measure global turbulence. The NetVIX multiplicatively decomposes into an average volatility and a network amplifier index (the degree to which market risk are amplified via a web of interconnectedness). It additively decomposes into marginal volatility indices for measuring individual contribution to global turmoil. The NetVIX is shown to be a novel approach to measuring global market risk, and an alternative to the VIX.

The empirical application presents a study of the relationship between the interconnectedness among 20 major stock markets and global market risk over the last two decades. The result shows that dense interconnectedness increases market vulnerability, thereby confirming the findings of Billio et al. (2012) and Blume et al. (2013). We document evidence of a significant relationship between the NetVIX and the VIX, with both indices providing similar signals about the direction of global market risk. We show that the average market volatilities and the network amplifier index record their historic highest spikes during the global financial crisis and the COVID pandemic, indicating strong contagion in the equities market during these periods. We show that during crisis periods (when average market volatility is usually higher than 75th percentile), the network of financial interconnectedness amplifies market risk more than 700 percent to cause a global meltdown. Also during crisis times, the level of risk is relatively higher and more persistent in some markets (like the US, Germany, and France) than others (like Hong Kong and Japan), which implies market losses for investors already with long exposures. Finally, the results reveal that the highest risk-contributing markets to global meltdown are the US, Brazil, Hong Kong, France, and Germany.

References

Acemoglu, D., A. Ozdaglar, and A. Tahbaz-Salehi (2015). Systemic Risk and Stability in Financial Networks. *American Economic Review 105*(2), 564–608.

Adrian, T. and M. K. Brunnermeier (2016). CoVaR. *The American Economic Review 106*(7), 1705–1741.

Ahelegbey, D. F., M. Billio, and R. Casarin (2016a). Bayesian Graphical Models for Structural Vector Autoregressive Processes. *Journal of Applied Econometrics 31*(2), 357–386.

Ahelegbey, D. F., M. Billio, and R. Casarin (2016b). Sparse Graphical Vector Autoregression: A Bayesian Approach. *Annals of Economics and Statistics 123/124*, 333–361.

Allen, F. and D. Gale (2000). Financial Contagion. *Journal of Political Economy 108*(1), 1–33.

Avdjiev, S., P. Giudici, and A. Spelta (2019). Measuring Contagion Risk In International Banking. *Journal of Financial Stability 42*, 36–51.

Banulescu, G.-D. and E.-I. Dumitrescu (2015). Which are the SIFIs? A Component Expected Shortfall Approach to Systemic Risk. *Journal of Banking and Finance 50*, 575–588.

Barigozzi, M. and C. Brownlees (2019). NETS: Network Estimation for Time Series. *Journal of Applied Econometrics 34*(3), 347–364.

Basu, S. and G. Michailidis (2015). Regularized Estimation in Sparse High-dimensional Time Series Models. *The Annals of Statistics 43*(4), 1535–1567.

Battiston, S., D. Delli Gatti, M. Gallegati, B. Greenwald, and J. E. Stiglitz (2012). Liaisons Dangereuses: Increasing Connectivity, Risk Sharing, and Systemic Risk. *Journal of Economic Dynamics and Control 36*(8), 1121–1141.

Bianchi, D., M. Billio, R. Casarin, and M. Guidolin (2019). Modeling Systemic Risk with Markov Switching Graphical SUR Models. *Journal of Econometrics 210*(1), 58–74.

Billio, M., R. Casarin, and L. Rossini (2019). Bayesian Nonparametric Sparse VAR Models. *Journal of Econometrics 212*(1), 97–115.

Billio, M., M. Getmansky, A. W. Lo, and L. Pelizzon (2012). Econometric Measures of Connectedness and Systemic Risk in the Finance and Insurance Sectors. *Journal of Financial Economics 104*(3), 535 – 559.

Blume, L., D. Easley, J. Kleinberg, R. Kleinberg, and É. Tardos (2013). Network Formation in the Presence of Contagious Risk. *ACM Transactions on Economics and Computation 1*(2), 6.

Bonacich, P. (1972). Technique for Analyzing Overlapping Memberships. *Sociological Methodology 4*, 176–185.

Borgatti, S. P. and M. G. Everett (2006). A Graph-Theoretic Perspective on Centrality. *Social Networks 28*(4), 466–484.

Brownlees, C. and R. F. Engle (2017). SRISK: A Conditional Capital Shortfall Measure of Systemic Risk. *The Review of Financial Studies 30*(1), 48–79.

Carvalho, C. M. and M. West (2007). Dynamic Matrix-Variate Graphical Models. *Bayesian Analysis 2*, 69–98.

Corander, J. and M. Villani (2006). A Bayesian Approach to Modelling Graphical Vector Autoregressions. *Journal of Time Series Analysis 27*(1), 141–156.

Diebold, F. X. and K. Yilmaz (2014). On the Network Topology of Variance Decompositions: Measuring the Connectedness of Financial Firms. *Journal of Econometrics 182*(1), 119–134.

Faust, K. (1997). Centrality in Affiliation Networks. *Social Networks 19*(2), 157–191.

Freeman, L. C. (1978). Centrality in Social Networks Conceptual Clarification. *Social Networks 1*(3), 215–239.

Freixas, X., B. M. Parigi, and J.-C. Rochet (2000). Systemic Risk, Interbank Relations, and Liquidity Provision by the Central Bank. *Journal of Money, Credit and Banking 32*(3), 611–638.

Geiger, D. and D. Heckerman (2002). Parameter Priors for Directed Acyclic Graphical Models and the Characterization of Several Probability Distributions. *Annals of Statistics 30*(5), 1412–1440.

Gelman, A. and D. B. Rubin (1992). Inference from Iterative Simulation Using Multiple Sequences, (with discussion). *Statistical Science 7*, 457–511.

George, E. I., D. Sun, and S. Ni (2008). Bayesian Stochastic Search for VAR Model Restrictions. *Journal of Econometrics 142*, 553–580.

Giudici, P. and A. Spelta (2016). Graphical Network Models for International Financial Flows. *Journal of Business and Economic Statistics 34*(1), 128–138.

Haldane, A. G. (2013). Rethinking The Financial Network. In *Fragile Stabilität–Stabile Fragilität*, pp. 243–278. Springer.

Härdle, W. K., W. Wang, and L. Yu (2016). TENET: Tail-Event driven NETwork risk. *Journal of Econometrics 192*(2), 499–513.

Huang, X., H. Zhou, and H. Zhu (2012). Systemic Risk Contributions. *Journal of Financial Services Research 42*(1-2), 55–83.

Kinlaw, W. and D. Turkington (2013). Correlation Surprise. *Journal of Asset Management 14*(6), 385–399.

Kock, A. B. and L. Callot (2015). Oracle Inequalities for High Dimensional Vector Autoregressions. *Journal of Econometrics 186*(2), 325–344.

Kritzman, M. and Y. Li (2010). Skulls, Financial Turbulence, and Risk Management. *Financial Analysts Journal 66*(5), 30–41.

Kritzman, M., Y. Li, S. Page, and R. Rigobon (2011). Principal Components as a Measure of Systemic Risk. *Journal of Portfolio Management 37*(4), 112.

Newman, M. (2010). *Networks: An Introduction.* Oxford University Press.

Roberts, G. O. and S. K. Sahu (1997). Updating Schemes, Covariance Structure, Blocking and Parametrization for the Gibbs Sampler. *Journal of the Royal Statistical Society 59*, 291 – 318.

Appendix A. Network Sampling Algorithm

Given some lag length $\hat{p}$, inference of the network is made feasible by integrating out other parameters analytically to obtain a marginal likelihood function over graphs (see Ahelegbey et al., 2016a; Geiger and Heckerman, 2002). Let $V_y = (y_i, \ldots, y_n)$ be the vector of indices of response variables, and $V_z = (z_1, \ldots, z_{n\hat{p}})$ the indices of the variables in Z. The network relationship from $z_\psi \in V_z$ to $y_i \in V_y$ can be represented by $(G_{y_i, z_\psi} = 1)$. Following Geiger and Heckerman (2002), the closed-form expression of the local marginal likelihood is given by

$$P(Y|G_{y_i,z_\psi}) = \frac{\pi^{-\frac{1}{2}N} \ \nu_0^{\frac{1}{2}\nu_0}}{\nu_n^{\frac{1}{2}\nu_n}} \frac{\Gamma\left(\frac{\nu_0+N-n_x}{2}\right)}{\Gamma\left(\frac{\nu_0-n_x}{2}\right)} \left(\frac{|Z'_\psi Z_\psi + \nu_0 I_{n_v}|}{|X'_i X_i + \nu_0 I_{n_x}|}\right)^{\frac{1}{2}\nu_n} \tag{A.1}$$

where $\Gamma(\cdot)$ is the gamma function, $X_i = (Y_i, Z_\psi)$, I_d is a d-dimensional identity matrix, n_ψ is the number of covariates in Z_ψ, $n_x = n_\psi + 1$, $\nu_0 > n_x$ is a degree of freedom hyper-parameter of the prior precision matrix of (Y, Z), and $\nu_n = \nu_0 + N$. Equation (A.1) indicates that only the ratio of the posterior sum of squares depend on the data. Thus, we reduce computational time by pre-computing the part of (A.1) that is independent of the data, for different values of $n_x \in [1, m]$ and for fixed $\nu_0 = m + 2$ and N. We also pre-compute the posterior of the full sum of squares matrix and extract the sub-matrices that relates to $\{Z_\psi\}$ and $\{(Y_i, Z_\psi)\}$. For computational details of the score function (see Ahelegbey et al., 2016a).

Algorithms 1 and 2 samples $[G_{1:\hat{p}}|Y, \hat{p}]$ and $[G_0|Y, \hat{G}_{1:\hat{p}}, \hat{p}]$, respectively, via a Metropolis-within-Gibbs scheme with random walk proposal. In a typical MCMC algorithm, the space exploration crucially depends on the choice of the starting point of the chain. Usually, a set of burn-in iteration is advanced to obtain a good starting point. We navigate around this problem by initializing the network search with a Granger-causality-like structure. More precisely, we examine whether the prediction of a response variable can be improved by incorporating information from each of the explanatory variables. The variables that pass this test are retained to provide a starting structure for the MCMC iteration, which is designed to sample the combination of explanatory variables that produce high-scoring networks.

Appendix A.1. Convergence and Mixing of MCMC

We examine the mixing of the chains generated by the Gibbs sampler for the samples of $G = \{G_{1:p}, G_0\}$. We monitor the mixing of the MCMC by computing the local log-likelihood score. We use the score to compute the potential scale reduction factor (PSRF) and multivariate PSRF (MPSRF) of Gelman and Rubin (1992). Following standard application, the MCMC chain is considered as converged if the PSRF and MPSRF are less than 1.2. With 50,000 sampled networks, we ensure that the convergence and mixing of the MCMC chains are tested with both PSRF and MPSRF satisfying the above-mentioned condition.

We estimate the posterior probability of the edges by averaging over the sampled networks, i.e., $\hat{\gamma}_{ij} = \frac{1}{H}\sum_{h=1}^{H} G_{i,j}^{(h)}$, where H is the total number of posterior samples of the graph. Due to the uncertainty in the network link determination, we consider a one-sided posterior

Algorithm 1 Sampling $[G_{1:\hat{p}}|Y, \hat{p}]$

Require: Set of responses $V_y = (y_i, \ldots, y_n)$ and lagged attributes $V_z = (z_1, \ldots, z_{n\hat{p}})$
Initialize $G^{(1)}_{1:\hat{p}} = \emptyset$
for $y_i \in V_y$ **do**
    for $z_j \in V_z$ **do**
        Compute $\phi_a = P(Y|G^{(1)}_{y_i,\emptyset|1:\hat{p}})$ and $\phi_b = P(Y|G^{(1)}_{y_i,z_j|1:\hat{p}})$
        if $\phi_b > \phi_a$ **then** $G^{(1)}_{y_i,z_j|1:\hat{p}} = 1$ **else** $G^{(1)}_{y_i,z_j|1:\hat{p}} = 0$

for $h = 2 : H$, (MCMC Iteration by performing local network update) **do**
    for $y_i \in V_y$, set $G^{(*)}_{y_i|1:\hat{p}} = G^{(h-1)}_{y_i|1:\hat{p}}$ **do**
        Randomly draw $z_k \sim V_z$
        Add/remove link from z_k to y_i: $G^{(*)}_{y_i,z_k|1:\hat{p}} = 1 - G^{(h-1)}_{y_i,z_k|1:\hat{p}}$
        Compute $\phi = \exp\left[\,\log P(Y|G^{(*)}_{y_i|1:\hat{p}}) - \log P(Y|G^{(h-1)}_{y_i|1:\hat{p}})\,\right]$. Draw $u \sim \mathcal{U}(0,1)$.
        if $u < \min\{1, \phi\}$ **then** $G^{(h)}_{y_i|1:\hat{p}} = G^{(*)}_{y_i|1:\hat{p}}$ **else** $G^{(h)}_{y_i|1:\hat{p}} = G^{(h-1)}_{y_i|1:\hat{p}}$

Algorithm 2 Sampling $[G_0|Y, \hat{G}_{1:\hat{p}}, \hat{p}]$

Require: Set of attributes $V_y = (y_i, \ldots, y_n)$ and estimated lag network $\hat{G}_{1:\hat{p}}$
Initialize $G^{(1)}_0 = \emptyset$ and $G^{(1)}_{0:\hat{p}} = [G^{(1)}_0, \hat{G}_{1:\hat{p}}]$
for $y_i \in V_y$ **do**
    Set $V_{y_i} = V_y \backslash \{y_i\}$ and $\{z_\pi : \hat{G}_{y_i,z_\pi|1:\hat{p}} = 1\}$
    for $y_j \in V_{y_i}$ **do**
        Set $\pi_i = (y_j \cup z_\pi)$. Compute $\phi_a = P(Y|G^{(1)}_{y_i,z_\pi|0:\hat{p}})$ and $\phi_b = P(Y|G^{(1)}_{y_i,\pi_i|0:\hat{p}})$
        if $\phi_b > \phi_a$ **then** $G^{(1)}_{y_i,\pi_i|0:\hat{p}} = 1$ **else** $G^{(1)}_{y_i,z_\pi|0:\hat{p}} = 1$

for $h = 2 : H$, (MCMC Iteration by performing local network update) **do**
    for $y_i \in V_y$, set $G^{(*)}_{y_i|0:\hat{p}} = G^{(h-1)}_{y_i|0:\hat{p}}$ **do**
        Randomly draw $y_k \sim V_{y_i}$
        Add/remove link from y_k to y_i: $G^{(*)}_{y_i,y_k|0:\hat{p}} = 1 - G^{(h-1)}_{y_i,y_k|0:\hat{p}}$
        Compute $\phi = \exp\left[\,\log P(Y|G^{(*)}_{i|0:\hat{p}}) - \log P(Y|G^{(h-1)}_{i|0:\hat{p}})\,\right]$. Draw $u \sim \mathcal{U}(0,1)$.
        if $u < \min\{1, \phi\}$ **then** $G^{(h)}_{y_i|0:\hat{p}} = G^{(*)}_{y_i|0:\hat{p}}$ **else** $G^{(h)}_{y_i|0:\hat{p}} = G^{(h-1)}_{y_i|0:\hat{p}}$

credibility interval for the edge posterior distribution. Following Ahelegbey et al. (2016a), we parameterize the ij-th entry of the estimate of $\hat{G}$ via a link function:

$$\hat{G}_{i,j} = \mathbf{1}(q_{ij} > 0.5), \qquad q_{ij} = \hat{\gamma}_{ij} - z_{(1-\alpha)}\sqrt{\frac{\hat{\gamma}_{ij}(1-\hat{\gamma}_{ij})}{n_{\text{eff}}}}, \qquad n_{eff} = \frac{H}{1 + 2\sum_{t=1}^{\infty}\rho_t} \tag{A.2}$$

where n_{eff} is the MCMC effective sample size of the network graph, ρ_t is the autocorrelation of the graph scores at lag t, and $z_{(1-\alpha)}$ is the z-score of the normal distribution at $(1-\alpha)$ significance level. A default value for α is 0.05 and $z_{(1-\alpha)} = 1.65$.